Highlights

Characterisation of a Timepix detector for use in SEM acceleration voltage range

Nikita Denisov,Daen Jannis,Andrey Orekhov,Knut Müller-Caspary,Johan Verbeeck

- Timepix DED shows excellent performance for SEM acceleration voltage range (15-30 keV) with near ideal results of PSF-MTF and reasonable DQE(0) of 60%.
- We observe PSF-MTF degradation with acceleration voltage increase and PSF-MTF improvements with the rise of detector threshold level.
- DQE values show a significant DQE reduction at increased detector threshold value.
- At acceleration voltage of 15 keV for both AdvaPix and Minipix lower values of DQE are obtained, this can be assumed to be the result of more pronounced interaction of Al contact layer on top of the sensor area with incoming electrons.

Characterisation of a Timepix detector for use in SEM acceleration voltage range

Nikita Denisov[a,*], Daen Jannis[a], Andrey Orekhov[a], Knut Müller-Caspary[b] and Johan Verbeeck[a]

[a]EMAT, University of Antwerp, Groenenborgerlaan 171, Antwerp, 2020, Belgium
[b]Ludwig-Maximilians-Universität München, Butenandtstr. 5-13, Munich, 81377, Germany

ARTICLE INFO

Keywords:
Timepix
Direct electron detector
Hybrid pixel detector
Detective Quantum Efficiency (DQE)
Modulation Transfer Function (MTF)
Single Spot Illumination
SEM

ABSTRACT

Hybrid pixel direct electron detectors are gaining popularity in electron microscopy due to their excellent properties. Some commercial cameras based on this technology are relatively affordable which makes them attractive tools for experimentation especially in combination with an SEM setup. To support this, a detector characterisation (Modulation Transfer Function, Detective Quantum Efficiency) of an Advacam Minipix and Advacam Advapix detector in the 15-30 keV range was made. In the current work we present images of Point Spread Function, plots of MTF / DQE curves and values of DQE(0) for these detectors. At low beam currents, the silicon detector layer behaviour should be dominant, which could make these findings transferable to any other available detector based on either Medipix2, Timepix or Timepix3 provided the same detector layer is used.

1. Introduction

Direct electron detectors (DED) combine high detector quantum efficiency (DQE), excellent signal to noise ratio and fast operation [1]. Therefore, it comes as no surprise that such devices already made their way in almost every advanced detection and imaging setup [2]. Initially these devices were intended for X-ray detection but specific setups for detecting visible light, UV, electrons, etc. have emerged and fueled progress in diverse areas of science [3], [4], [5]. The capability to directly detect electrons without the need for a scintillator has proven attractive in the domain of electron microscopy [6], [7], [8], [9]. Indeed, TEM setups can benefit significantly from DED technology as it offers:

- Beam hardness by separating the detector layer from the electronic readout circuitry.
- No added noise except for the inevitable counting noise.
- High detection efficiency. This is important to make every electron count in the many cases where beam damage is putting limits on what electron microscopy can achieve.
- Potential for event based readout (Timepix and Timepix3) offering intrinsic data reduction as the data scales with the actual information that is obtained in a per electron fashion.
- Intrinsic high time resolution reaching tens of kHz frame speeds (Medipix2) or few ns timing of individual electron detection events (Timepix3). This can be exploited for in situ time resolved experiments or real time 4D-STEM data acquisition [10], [11].
- Counting mode offers up to 24 bit dynamic range (Medipix3) which is highly attractive for capturing diffraction patterns and low loss EELS spectra [12]

On the downside, the limited number of pixels in a single chip can be mentioned (256x256 for Medipix2, Timepix, TimePix3) as well as the relatively large pixel size (55×55 μm). Some of these downsides can be overcome by tiling multiple readout chips together under a single larger detection layer, leaving some seam effects to take into account. In this respect other detector technologies can offer far higher pixel densities which can be important e.g. for imaging

*Corresponding author
nikita.denisov@uantwerpen.be (N. Denisov); jo.verbeeck@uantwerpen.be (J. Verbeeck)
ORCID(s): 0000-0003-4186-8415 (N. Denisov); 0000-0003-0285-0511 (D. Jannis); 0000-0002-7517-5484 (A. Orekhov); 0000-0002-2588-7993 (K. Müller-Caspary); 0000-0002-7151-8101 (J. Verbeeck)

applications. Another important downside is the somewhat limited electron current they can digest, as each event has to be transferred over a communication channel towards an field programmable gate array that takes care of repackaging and grouping the data and sending it over another communication channel towards e.g. a computer for storage [13]. This makes these detectors excellent for low dose experiments although their behaviour upon local saturation is in many ways superior as compared to scintillator based detectors.

Besides its gaining popularity in TEM, DEDs started to appear in SEM based setups as well [14], [15], [16] where their benefits are supposed to equally apply.

Regarding the detection layer in hybrid DEDs, doped Si is currently the most common material. Monte Carlo simulations of electron tracks in Si [17] predict that higher energy electron beams produce a wider spatial spread deposited on the detector by the incident electron. Typical TEM acceleration voltages of 100-300 keV create a spatial spread that exceeds the size of one pixel thus blurring the detected image. In SEM, accelerating voltages are typically lower (1-30 keV) and DED's should perform even better in such conditions. To evaluate this point we examined the modulation transfer function (MTF) and detective quantum efficiency (DQE) of two commercially available hybrid pixel DED's based on a Timepix sensor chip in a SEM setup in the range of 15-30 keV incident beam energy.

2. Materials and methods

Investigated detectors are Advacam MiniPix and Advacam AdvaPix equipped with Timepix chip [18, 19]. The detector layer is nominally 300 μm thick Si covered with a thin layer of Al and bump bonded on top of readout electronics. The chip provides 256x256 pixels of 55 μm size. The cameras provide a threshold setting that determines above which level of current pulse from the detector layer a detection event is fired. This relates to setting a threshold on the energy of incoming particles to be detected. Particles with energies below this threshold are ignored.

Experiments were performed on a Tescan Mira FEG SEM. Data process and control of the experiment is made entirely through Python accessing both microscope, camera and piezo motors through well defined APIs. Piezo stage assembled for this experiment consists of 2 Xeryon linear piezo motors with encoder resolution of 312 nm arranged in XY configuration. Beam current values were verified using Keithley 6485 picoammeter connected to custom built retractable Faraday cup.

2.1. MTF measurement

By definition, the MTF can be obtained from the Point Spread Function (PSF) by doing a Fourier transform [20] :

$$MTF(\vec{\omega}) = FT(PSF(\vec{r})) \tag{1}$$

where $\vec{\omega}$ is spatial frequency, FT - Fourier transform and $\vec{r}$ the 2D coordinate in the detector plane.

Contrary to (scintillator coupled) charge coupled devices (CCD)'s, hybrid pixel direct electron detectors have the benefit of being beam hard and have relatively large pixel sizes (55 μm in our case). This allows to illuminate the detector with a considerable beam current without detector degradation and a single spot illumination method [21] can be used to determine the PSF directly. In an ideal case we would converge the beam in the area of a single detector pixel and extract the PSF directly from the detector output. In reality, converging the beam into a single pixel on the investigated detectors even at the lowest beam current settings leads to saturation of the pixel value and yields no meaningful results as the electron dose per pixel is too high [17]. A solution to this is increasing the beam spot diameter by defocusing the objective lens of the SEM and cutting it with a mechanical aperture that projects a beam of size less than size of a detector pixel. This results in a significant reduction of beam current which can be controlled by the ratio of beam area to aperture area. We used a commercial ThermoFisher scientific strip - aperture of 16 μm diameter (part # 4035.273.67441) and mounted it on a Xeryon XY linear piezo stage placed 5 mm above the detector plane as sketched in Figure 1.

The initial position of the aperture selected beam with respect to the sensor pixel array is unknown. To obtain sufficient statistics, the aperture is moved by the XY piezo stage in a snake-like pattern in a way that the whole area of a pixel is scanned by the projected circular beam. The aperture movement is small compared to the incoming electron beam size and the intensity is homogeneous over the area of movement to make sure that the beam current on the detector does not change during the experiment. The scanned area is a square around 80 μm with an aperture defined beam size of 16 μm. This way we can say for sure that at least one pixel is completely covered with electron beam. This scanning procedure is repeated for hundred pixels located in different positions in sensor to get better statistics. Alternatively, one could perform the scanning motion in the detector plane [21] instead of moving the incoming beam.

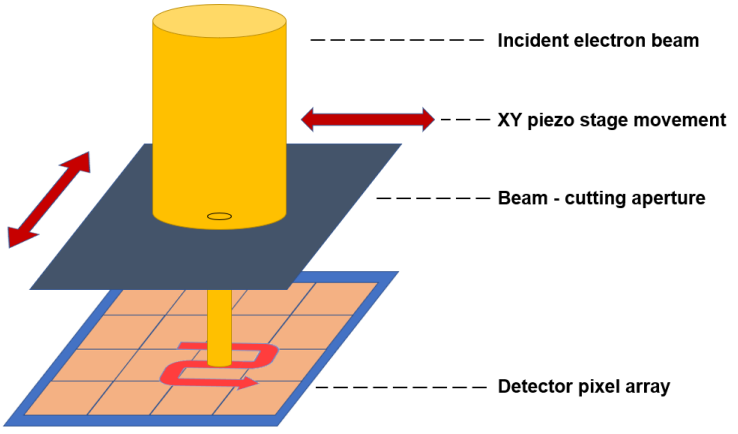

Figure 1: Experimental set-up for single spot illumination MTF measurement.

The individual frames are then combined to generate an average point spread function. Subsequently, the central pixel of the PSF was identified (the pixel with the highest count value). As the focus of this investigation is on the PSF of a single pixel, each frame was re-analyzed individually to exclude those frames where the intensity of neighboring pixels surrounding the previously determined PSF central pixel was greater than the central pixel itself. This selection criterion was applied to eliminate the signal spread contribution resulting from the accidental illumination in between two pixels, while retaining only the spread that is caused by the intrinsic characteristics of the detector. Afterwards selected frames are summed up again and the resulting PSF is retrieved.

MTF was derived by subjecting the PSF frame to a Fourier transform. To obtain a greater range of spatial frequencies in reciprocal space, the PSF frame was upsampled by a factor of 11 through the replacement of each single pixel in the frame with an 11x11 pixel array of equal intensity prior to the Fourier transform. Furthermore, a one-dimensional MTF curve was generated by calculating the rotational average of the resulting Fourier transform.

2.2. DQE measurement

2.2.1. DQE(0) measurement

DQE(0) can be calculated as the ratio between the number of detected electrons and the amount of incident electrons multiplied by a correction coefficient [22]:

$$DQE(0) = C\frac{n_{detect}}{n_{input}} = \frac{< m >}{< m^2 >}\frac{n_{detect}}{n_{input}} \tag{2}$$

where $< m >$ is average electron multiplicity (see section 2.2.2).

To calculate the value of DQE(0) first we need to confirm the amount of electrons that is incident on the detector plane. To do so we utilize a custom built Faraday cup combined with Keithley 6485 picoammeter to measure the beam current. Next, the beam spot size is decreased in a way to completely fit the beam in the detector sensor area dimensions. Detector acquisition (exposure) time is set to an appropriate value to avoid the saturation of individual pixels. The amount of detected electrons per second is then obtained as the sum of detected electrons in all pixels divided by the exposure time:

$$n_{detect} = \frac{n_{total}}{t_{exposure}} \tag{3}$$

To improve statistics, the amount of detected electrons per frame was averaged over forty thousand frames.
Then the amount of incident electrons is calculated as:

$$n_{input} = \frac{I_{beam} * t_{exposure}}{e_{el}} \tag{4}$$

where I_{beam} is beam current and e_{el} is the absolute value of electron charge.
Knowing n_{detect} and n_{input} DQE(0) can be obtained via (2)

2.2.2. Clustersize estimation

One electron can produce false counts by activating several (neighbouring) pixels [10], [23], [24]. This can happen if for example an electron lands directly in between pixels or if the electron inelastically scatters sideways after penetrating material causing activation of pixels along electron's trajectory given the energy is sufficient. Further we will call this agglomerates of false-activated pixels clusters. Presence of these clusters can lead to overoptimistic DQE(0) values that in principle can surpass 100%, complicating the determination of the actual detector behaviour. To negotiate this problem, separate measurement of average cluster size (electron multiplicity) [22] is carried out for each acceleration voltage and detector threshold in a semi-single electron experiment and a correction coefficient C is applied to the DQE(0) (see Eq. 2).

$$C = \frac{< m >}{< m^2 >}; < m >= \frac{\sum_{i=1}^{\infty} i N_i}{\sum_{i=1}^{\infty} N_i}; < m^2 >= \frac{\sum_{i=1}^{\infty} i^2 N_i}{\sum_{i=1}^{\infty} N_i} \tag{5}$$

where i is the amount of pixels (cluster size) lit by single incident electron and N_i is number clusters with i pixel size present on the detected frame.

As it is impossible to make stochastic electron sources emit strictly one electron at a time without going to extremely low temperatures we tried to get as close as possible to such conditions in semi single-electron mode by using the lowest detector exposure time (1 μs in our case) and widest beam spread (largest beam spot-size) resulting in an average dose of 0.00127 electrons per μs per pixel.

2.2.3. NPS measurement

The noise power spectrum (NPS) is calculated as the averaged value of the modulus square of a Fourier transform of a high number of homogeneously illuminated (flat field) frames. In order to reduce the error from slightly inhomogeneous illumination, we use image differences Δ_i between consecutive frames divided by a factor of 2 to obtain the NPS equivalent of a single image [20].

$$\Delta_i = \frac{Frame_{i+1} - Frame_i}{2} \tag{6}$$

Then the squared modulus is taken from a Fourier transform of the difference between resulting Δ_i frame and it's average intensity value $\overline{\Delta_i}$.

$$NPS_i(\omega) = \left| FT\left(\Delta_i - \overline{\Delta_i}\right)\right|^2 \tag{7}$$

The NPS is determined by averaging a high number of NPS_i. The NPS is converted from a 2D matrix to 1D NPS curve by radial averaging. Finally the resulting curve is fitted by a sinc function:

$$f_{sinc}(\omega) = [S_1 - S_2 * sinc(S_3\omega)]e^{-S_4^2\omega^2} \tag{8}$$

where S_i are the parameters to be found. In our case we used a non-linear least squares algorithm to make the fit and determine S_i.

2.2.4. DQE calculation

Having values of DQE(0), clustersize, MTF(ω) and NPS(ω) it is possible to calculate DQE(ω) [25] with the following equation :

$$DQE(w) = DQE(0)\frac{MTF^2(w)}{NPS(w)} \tag{9}$$

3. Results

In the following section we present results obtained with both AdvaCam AdvaPix and MiniPix detectors. As the trends show very similar behaviour we decided to show complete results for the Advapix only while the Minipix results are represented in supplementary information.

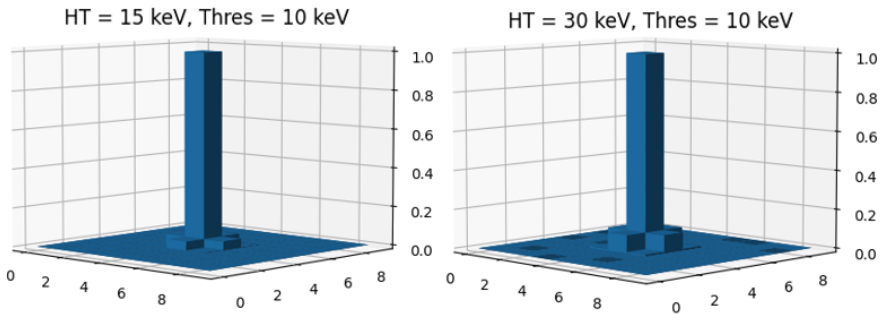

(a) Acceleration voltage effect

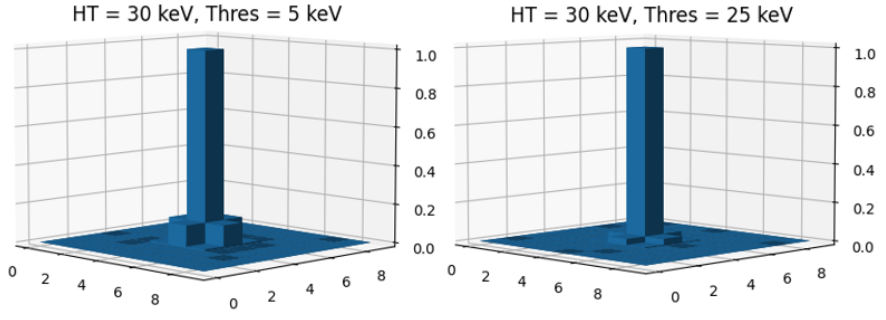

(b) Detector threshold effect

Figure 2: Point Spread Function of AdvaPix detector with Timepix sensor chip. Dependencies on a) acceleration voltage for constant detector threshold of 10 keV, b) detector threshold for constant acceleration voltage of 30 keV for AdvaPix detector are presented.

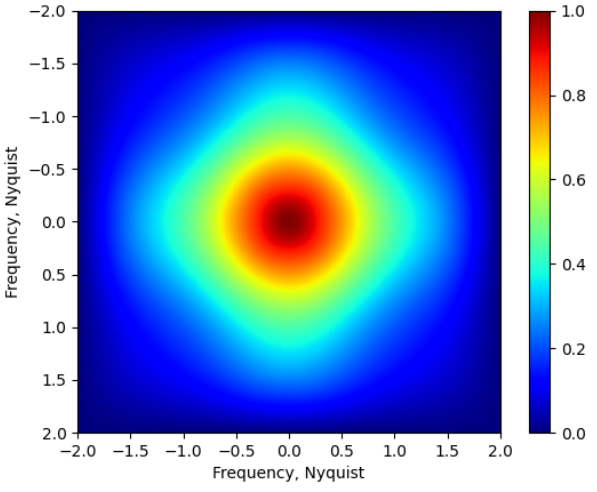

Figure 3: Modulation Transfer Function 2D plot of AdvaPix detector with Timepix sensor chip obtained for 15keV acceleration voltage with 10 keV detector threshold.

4. Discussion

The results show almost ideal MTF and PSF behaviour. PSF peaks presented in Figure 2 have minor deviation in the nearest neighboring pixels with respect to a single dirac delta as expected for an ideal square pixel response. This result is the expected outcome for this detection principle and the leakage into neighbouring pixels is entirely due to the scattering inside the detector layer which is relatively minor for low energy electron beams tested here. Acceleration

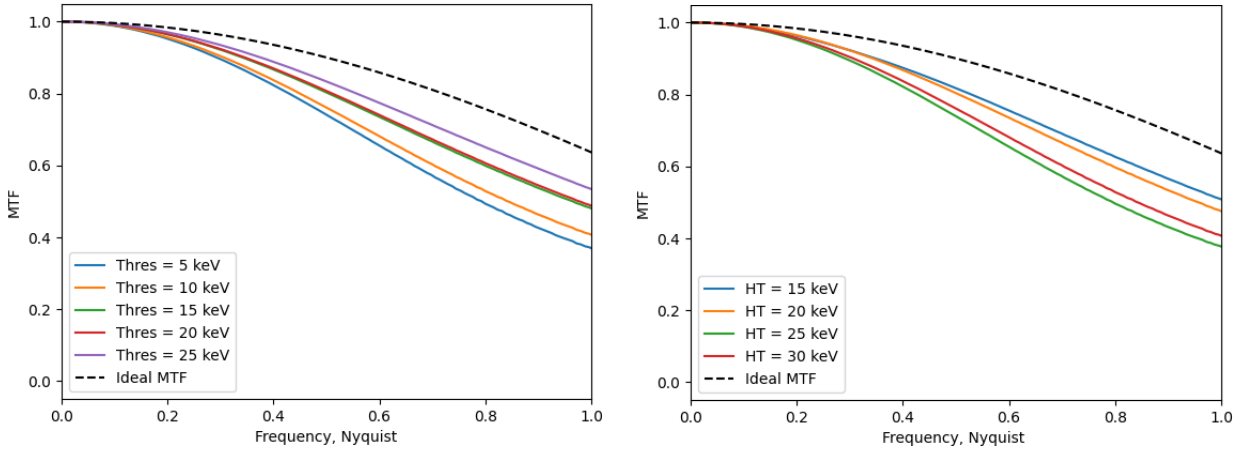

(a) Detector threshold effect @ 30 keV

(b) Acceleration voltage effect @ 10 keV threshold

Figure 4: Modulation Transfer Function rotational average curves of AdvaPix detector with Timepix sensor chip. Effect of: a) detector threshold on MTF with constant acceleration voltage of 30 keV b) acceleration voltage on MTF with constant detector threshold of 10 keV. MiniPix detector results can be found in supplementary info.

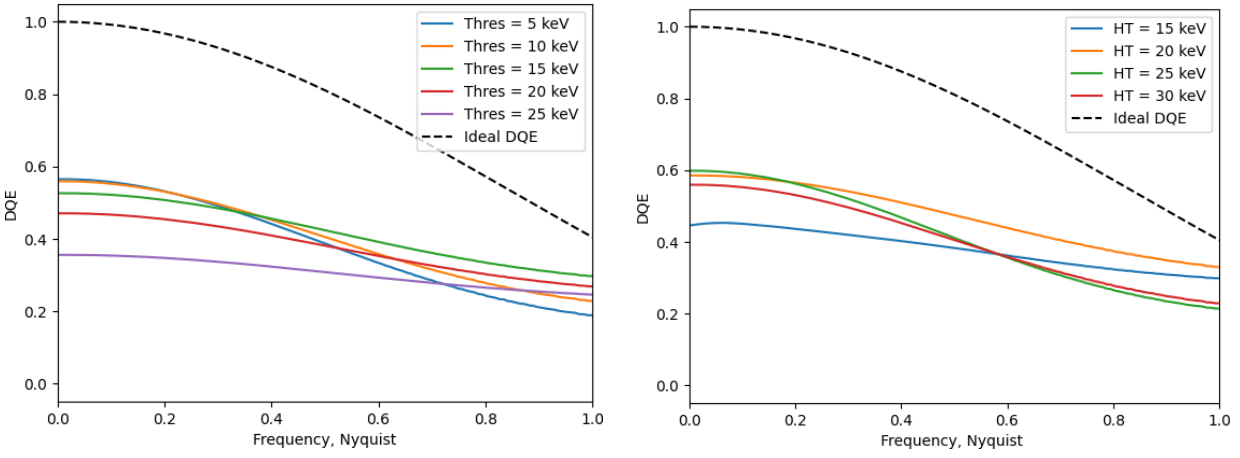

(a) Detector threshold effect @ 30 keV

(b) Acceleration voltage effect @ 10 kV thresh.

Figure 5: Detective Quantum Efficiency of AdvaPix detector with Timepix sensor chip. Effect of: a) detector threshold on DQE with constant acceleration voltage of 30 keV b) acceleration voltage on DQE with constant detector threshold of 10 keV. MiniPix detector results can be found in supplementary info.

voltage increase while keeping a constant detector threshold shown in Figure 2a, leads to a broadening of the PSF in line with increased sideways scattering throughout the thickness of the detector layer. Increasing the threshold voltage can partially compensate for this effect as on average electrons that have scattered further sideways have already lost more energy and can be discriminated. It is seen from Figure 2b that the closer the detector threshold tends to the acceleration voltage, the closer PSF peak resembles ideal square pixel response. This, affects however the amount of detected electrons and will deteriorate the DQE(0) up to the point where no electrons are detected if the threshold is chosen higher than the acceleration voltage. We found that the best ratio between PSF quality and intensity is setting the threshold approximately 60-70% of acceleration voltage.

The MTF, being obtained as the Fourier Transform of the PSF, follows a related trend. From Figure 4 one can find MTF curves that are very close to the theoretical limit for an ideal detector with square pixels. The general trend in acceleration voltage and threshold dependency remains the same as with PSF: higher values of acceleration voltage

Table 1
Advacam AdvaPix Timepix sensor DQE(0) values for different acceleration voltages and detector thresholds

		Detector threshold, keV				
		5	10	15	20	25
HT, keV	15	0.646	0.446	-	-	-
	20	0.697	0.585	0.436	-	-
	25	0.653	0.598	0.519	0.399	-
	30	0.565	0.560	0.526	0.471	0.356

Table 2
Advacam Minipix Timepix sensor DQE(0) values for different acceleration voltages and detector thresholds

		Detector threshold, keV				
		5	10	15	20	25
HT, keV	15	0.507	0.252	-	-	-
	20	0.665	0.508	0.286	-	-
	25	0.653	0.583	0.460	0.258	-
	30	0.554	0.551	0.496	0.381	0.188

lower the MTF towards higher spatial frequencies and increasing the detector threshold helps to counter this at the expense of detector quantum efficiency.

The effect of detector threshold on DQE can be clearly seen in Figure 5a. We observe a distinct change in the amount of detected electrons depending on threshold chosen. Indeed elevating the threshold value increases the range of discriminated electrons resulting in significant drop of DQE. This may be the crucial drawback for samples that degrade under electron beam as for such objects every undetected electron damages sample but does not provide information in the end. However, for samples where beam damage does not occur, the drop in DQE is not a big issue as detector noise is close to none. Analogous dependencies of MTF and DQE on detector threshold were presented in [23] for the range 60-80 keV with a Medipix3 chip.

In Figure 5b the dependence of DQE on accelerating voltage for a given threshold can be found. It is seen that all DQE curves with the exception of 15 keV are rather close to each other. Still some trends can be observed such as an increase of DQE with increasing accelerating voltage. This can be understood as higher energy electrons can more easily penetrate the inactive top sensor surface and produce also more electron hole pairs which makes it easier to detect the event. Moreover the amount of electrons that are completely repelled (backscattered) from the sensor material decreases with an increase of acceleration voltage. On the other hand, higher beam energies lead to more spatial spreading and therefore suppress the higher frequency part of the DQE curves. Correcting this by estimating clustering also becomes more difficult as there is a higher chance that clusters from separate events can merge into one big cluster with multiple centers of mass making it almost impossible to truthfully determine cluster size of the individual event. Another issue with cluster size correction could arise from the fact that more false-counts emerge due to a higher number of electrons landing in closer proximity to each other than in single-electron mode measurements (discussed in section 2.2.1 and 2.2.2) as we reduce beam size to confine the whole beam on the sensor area for the DQE(0) study in a pursuit to collect every incident electron while in single-electron measurements the beam spread is maximal (exceeding detector dimensions) and distance between landing electrons is greater.

A maximum DQE(0) of approximately 60% was achieved on the AdvaPix detector for a threshold of 5 keV and accelerating voltage of 20 keV. We have acquired lower values of DQE (see tables 1, 2) at HT of 15 keV for both AdvaPix and Minipix. This can be assumed to be the result of more pronounced interaction of the Al contact layer on the top of sensor area with incoming electrons. In addition to this decrease in accelerating voltage makes backscatter electrons to occur more frequently.

Looking at tables 1, 2 DQE(0) results of AdvaPix and MiniPix camera show close resemblance to each other for values of detector thresholds that are much less than acceleration voltage. The difference in DQE(0) at detector thresholds that approach the incident beam energy values might be the outcome of higher noise level in some analog parts of MiniPix device, deviation in threshold calibration of devices and/or difference in sensor top contact bias

voltages. The MTF on the other hand seems to be unaffected by this difference and both devices show an almost identical result. Relevant figures can be found in supplementary info.

5. Conclusions

In this study we have performed a detailed characterization of two commercial hybrid pixel direct electron detectors based on a timepix sensor chip: AdvaCam AdvaPix and MiniPix with 300 μm Si detector layer and 55 μm pixels in the acceleration voltage range 15-30 keV. We have observed PSF-MTF degradation with acceleration voltage increase and PSF-MTF improvements with the rise of detector threshold level. Acquired DQE values show a significant DQE reduction at increased detector threshold values. We have confirmed timepix DED excellent performance for SEM acceleration voltage range (15-30 keV) with near ideal results of PSF-MTF and reasonable DQE(0) making it an attractive tool for experimentation in SEM because of its small size and relatively low cost. The results presented here form an indispensable basis for all researchers that want to utilise these and related cameras with the same 300 μm Si detector layer for electron beams in this range of acceleration voltages.

6. Acknowledgements

The authors acknowledge the financial support of the Research Foundation Flanders (FWO, Belgium) project SBO S000121N. The authors are grateful to Dr. Lobato for productive discussion of methods.

CRediT authorship contribution statement

Nikita Denisov: Conceptualization, Methodology, Software, Hardware, Experimental. **Daen Jannis:** Methodology. **Andrey Orekhov:** Methodology, technical support. **Knut Müller-Caspary:** Methodology, Software. **Johan Verbeeck:** Supervision,Conceptualization, Methodology.

References

[1] R Clough, Grigore Moldovan, and Angus Kirkland. Direct detectors for electron microscopy. *Journal of Physics: Conference Series*, 522:012046, 06 2014.

[2] Barnaby D A Levin. Direct detectors and their applications in electron microscopy for materials science. *Journal of Physics: Materials*, 4(4):042005, jul 2021.

[3] A.S. Tremsin and J.V. Vallerga. Unique capabilities and applications of microchannel plate (mcp) detectors with medipix/timepix readout. *Radiation Measurements*, 130:106228, 2020.

[4] J. Vallerga, Jason McPhate, Bettina Mikulec, Anton Tremsin, Allan Clark, and O. Siegmund. Noiseless imaging detector for adaptive optics with khz frame rates. *Proceedings of SPIE - The International Society for Optical Engineering*, 5490, 10 2004.

[5] R. van Gastel, I. Sikharulidze, S. Schramm, J.P. Abrahams, B. Poelsema, R.M. Tromp, and S.J. van der Molen. Medipix 2 detector applied to low energy electron microscopy. *Ultramicroscopy*, 110(1):33–35, 2009.

[6] G. McMullan, A.R. Faruqi, and R. Henderson. Chapter one - direct electron detectors. In R.A. Crowther, editor, *The Resolution Revolution: Recent Advances In cryoEM*, volume 579 of *Methods in Enzymology*, pages 1–17. Academic Press, 2016.

[7] A.R. Faruqi, D.M. Cattermole, R. Henderson, B. Mikulec, and C. Raeburn. Evaluation of a hybrid pixel detector for electron microscopy. *Ultramicroscopy*, 94(3):263–276, 2003.

[8] Anna-Clare Milazzo, Philippe Leblanc, Fred Duttweiler, Liang Jin, James C. Bouwer, Steve Peltier, Mark Ellisman, Fred Bieser, Howard S. Matis, Howard Wieman, Peter Denes, Stuart Kleinfelder, and Nguyen-Huu Xuong. Active pixel sensor array as a detector for electron microscopy. *Ultramicroscopy*, 104(2):152–159, 2005.

[9] Liang Jin, Anna-Clare Milazzo, Stuart Kleinfelder, Shengdong Li, Philippe Leblanc, Fred Duttweiler, James C. Bouwer, Steven T. Peltier, Mark H. Ellisman, and Nguyen-Huu Xuong. Applications of direct detection device in transmission electron microscopy. *Journal of Structural Biology*, 161(3):352–358, 2008. The 4th International Conference on Electron Tomography.

[10] D. Jannis, C. Hofer, C. Gao, X. Xie, A. Béché, T.J. Pennycook, and J. Verbeeck. Event driven 4d stem acquisition with a timepix3 detector: Microsecond dwell time and faster scans for high precision and low dose applications. *Ultramicroscopy*, 233:113423, 2022.

[11] Colin Ophus. Four-dimensional scanning transmission electron microscopy (4d-stem): From scanning nanodiffraction to ptychography and beyond. *Microscopy and Microanalysis*, 25(3):563–582, 2019.

[12] Marcel Tencé, Jean-Denis Blazit, Xiaoyan Li, Matus Krajnak, Eduardo Busto, Richard Skogeby, Léo Cambou, Mathieu Kociak, Odile Stéphan, and Alexandre Gloter. Electron energy-loss spectroscopy using merlinem - medipix3 detector. *Microscopy and Microanalysis*, 26:1–3, 07 2020.

[13] CERN. Medipix and Timepix detector chips specifications. `https://medipix.web.cern.ch/collaborations`, 2022. [Online; accessed 11-December-2022].

[14] A. Orekhov, D. Jannis, N. Gauquelin, G. Guzzinati, A. Nalin Mehta, S. Psilodimitrakopoulos, L. Mouchliadis, P. K. Sahoo, I. Paradisanos, A. C. Ferrari, G. Kioseoglou, E. Stratakis, and J. Verbeeck. Wide field of view crystal orientation mapping of layered materials, 2020.

[15] S. Vespucci, A. Winkelmann, G. Naresh-Kumar, K. P. Mingard, D. Maneuski, P. R. Edwards, A. P. Day, V. O'Shea, and C. Trager-Cowan. Digital direct electron imaging of energy-filtered electron backscatter diffraction patterns. *Phys. Rev. B*, 92:205301, Nov 2015.

[16] Miroslav Slouf, Radim Skoupy, Ewa Pavlova, and Vladislav Krzyzanek. Powder nano-beam diffraction in scanning electron microscope: Fast and simple method for analysis of nanoparticle crystal structure. *Nanomaterials*, 11(4), 2021.

[17] Mark W. Tate, Prafull Purohit, Darol Chamberlain, Kayla X. Nguyen, Robert Hovden, Celesta S. Chang, Pratiti Deb, Emrah Turgut, John T. Heron, Darrell G. Schlom, and et al. High dynamic range pixel array detector for scanning transmission electron microscopy. *Microscopy and Microanalysis*, 22(1):237–249, 2016.

[18] AdvaCam. AdvaPix - AdvaCam Fast Spectral Photon Counting Cameras. https://advacam.com/advapix, 2023. [Online; accessed 05-January-2023].

[19] AdvaCam. MiniPix - AdvaCam Portable Photon Counting Cameras Miniaturised. https://advacam.com/minipix, 2023. [Online; accessed 05-January-2023].

[20] Rachel S. Ruskin, Zhiheng Yu, and Nikolaus Grigorieff. Quantitative characterization of electron detectors for transmission electron microscopy. *Journal of Structural Biology*, 184(3):385–393, 2013.

[21] Axel Lubk, Falk Röder, Tore Niermann, Christophe Gatel, Sebastien Joulie, Florent Houdellier, César Magén, and Martin J. Hÿtch. A new linear transfer theory and characterization method for image detectors. part ii: Experiment. *Ultramicroscopy*, 115:78–87, 2012.

[22] T. Michel, G. Anton, M. BÃ¶hnel, J. Durst, M. Firsching, A. Korn, B. Kreisler, A. Loehr, F. Nachtrab, D. NiederlÃ¶hner, F. Sukowski, and P. Takoukam Talla. A fundamental method to determine the signal-to-noise ratio (snr) and detective quantum efficiency (dqe) for a photon counting pixel detector. *Nuclear Instruments and Methods in Physics Research Section A: Accelerators, Spectrometers, Detectors and Associated Equipment*, 568(2):799–802, 2006.

[23] J.A. Mir, R. Clough, R. MacInnes, C. Gough, R. Plackett, I. Shipsey, H. Sawada, I. MacLaren, R. Ballabriga, D. Maneuski, V. O'Shea, D. McGrouther, and A.I. Kirkland. Characterisation of the medipix3 detector for 60 and 80kev electrons. *Ultramicroscopy*, 182:44–53, 2017.

[24] G. McMullan, D.M. Cattermole, S. Chen, R. Henderson, X. Llopart, C. Summerfield, L. Tlustos, and A.R. Faruqi. Electron imaging with medipix2 hybrid pixel detector. *Ultramicroscopy*, 107(4):401–413, 2007.

[25] Rüdiger R. Meyer and Angus I. Kirkland. Characterisation of the signal and noise transfer of ccd cameras for electron detection. *Microscopy Research and Technique*, 49(3):269–280, 2000.

Supplement to Characterisation of a Timepix detector for use in SEM voltage range

1 Minipix MTF and DQE figures

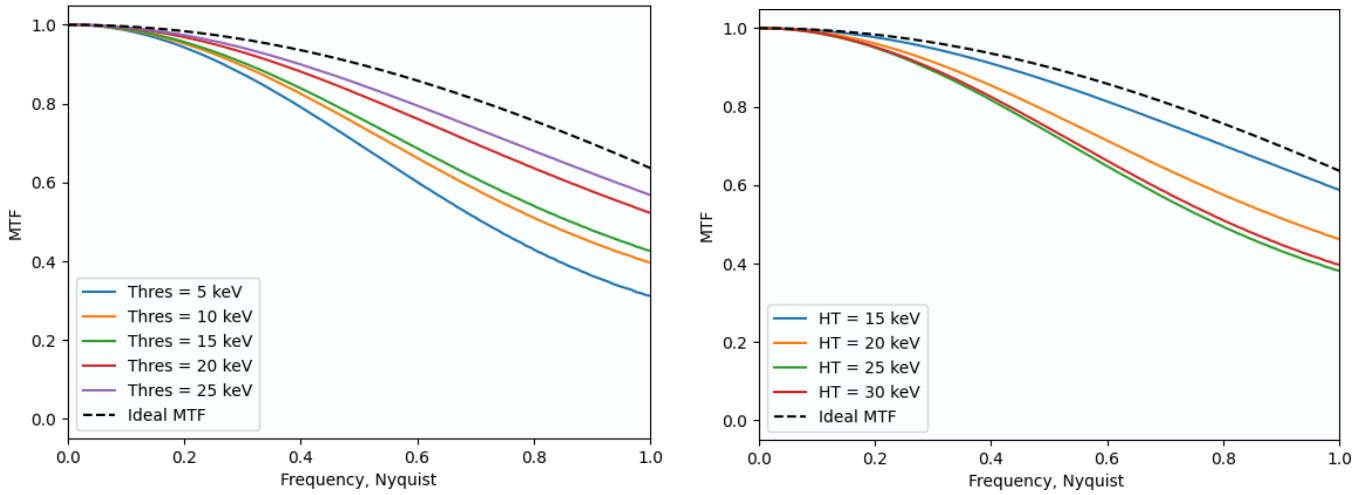

(a) Detector threshold effect @ 30 keV

(b) Acceleration voltage effect @ 10 keV threshold

Figure 1: Modulation Transfer Function rotational average curves of MiniPix detector with Timepix sensor chip. Effect of: a) detector threshold on MTF with constant acceleration voltage of 30 keV b) acceleration voltage on MTF with constant detector threshold of 10 keV.

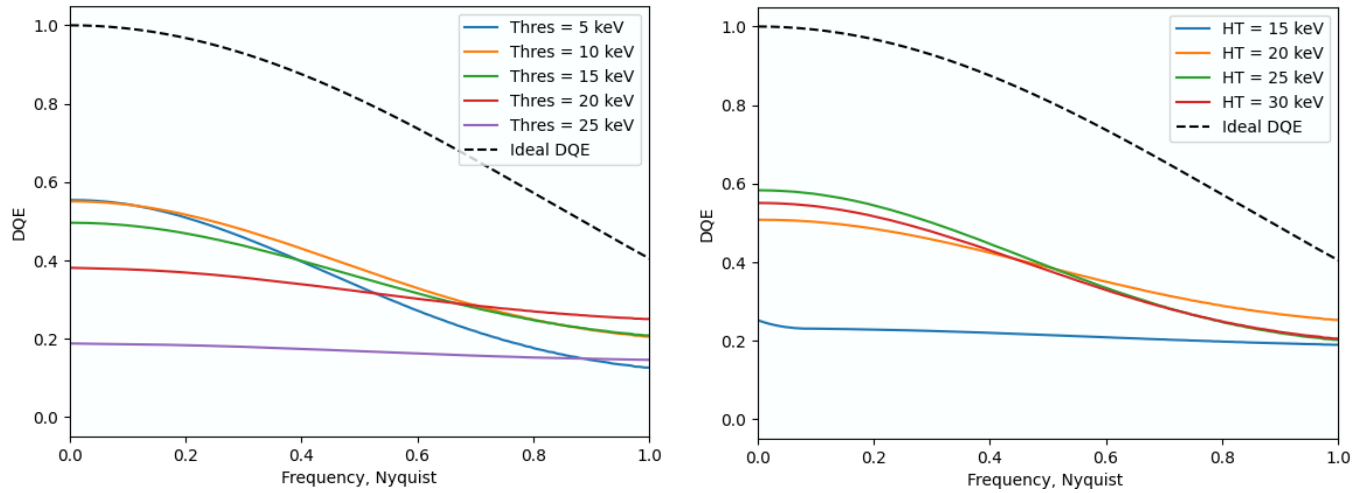

(a) Detector threshold effect @ 30 keV

(b) Acceleration voltage effect @ 10 kV thresh.

Figure 2: Detective Quantum Efficiency of MiniPix detector with Timepix sensor chip. Effect of: a) detector threshold on DQE with constant acceleration voltage of 30 keV b) acceleration voltage on DQE with constant detector threshold of 10 keV.